Electronic Supplementary Material (ESI) for ChemComm.

Supplementary Information:

On-Surface Synthesis of Heptacene on Ag(001) from Brominated and Non-Brominated Tetrahydroheptacene Precursors.

Luciano Colazzo,[a,b] Mohammed S. G. Mohammed,[a,b] Ruth Dorel,[c] Pawel Nita, [a,b] Carlos García Fernández,[a] Paula Abufager,[d] Nicolás Lorente,[a,b] Antonio Echavarren,[c,e] and Dimas G. de Oteyza *[a,b,f]

[a] Donostia International Physics Center (DIPC), 20018 San Sebastián, Spain.

[b] Centro de Física de Materiales (CSIC-UPV/EHU) - MPC, 20018 San Sebastián, Spain.

[c] Institute of Chemical Research of Catalonia (ICIQ), Barcelona Institute of Science and Technology, 43007 Tarragona, Spain.

[d] Instituto de Física de Rosario, Consejo Nacional de Investigaciones Científicas y Técnicas (CONICET) and Universidad Nacional de Rosario, (2000) Rosario, Argentina

[e] Departament de Química Orgànica i Analítica, Universitat Rovira i Virgili, 43007 Tarragona, Spain

[f] Ikerbasque, Basque Foundation for Science, 48011 Bilbao, Spain.

Precursor synthesis

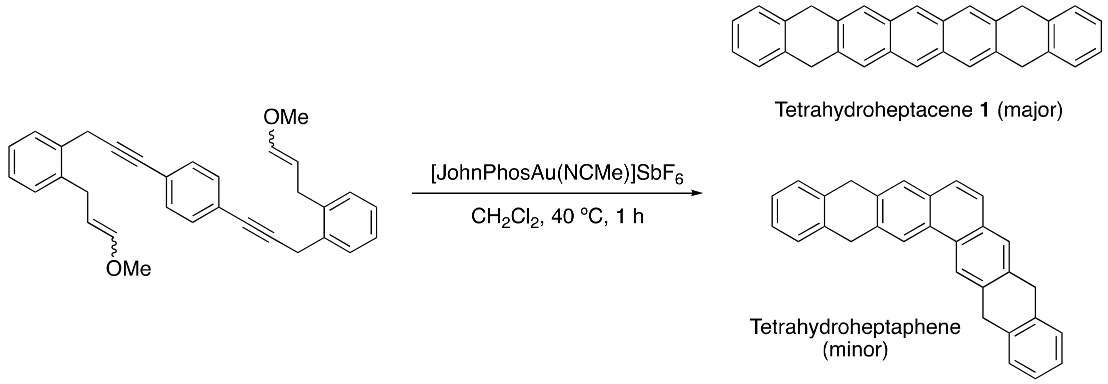

Scheme S1. The sample containing a mixture of tetrahydroheptacene (**1**) and kinked tetrahydroheptaphene was obtained by following the procedure reported for the preparation of **1**[1] with a modified purification protocol. Thus, the crude mixture was washed and centrifuged with MeOH (2x5 mL) and a 4:1 *v/v* MeOH:CH$_2$Cl$_2$ mixture (5 mL). The remaining solid was subsequently dried under reduced pressure to afford a white solid that consists of **1** as the major product together with minor amounts of kinked tetrahydroheptaphene.

Determination of the position of hydrogenated rings from conventional STM imaging.

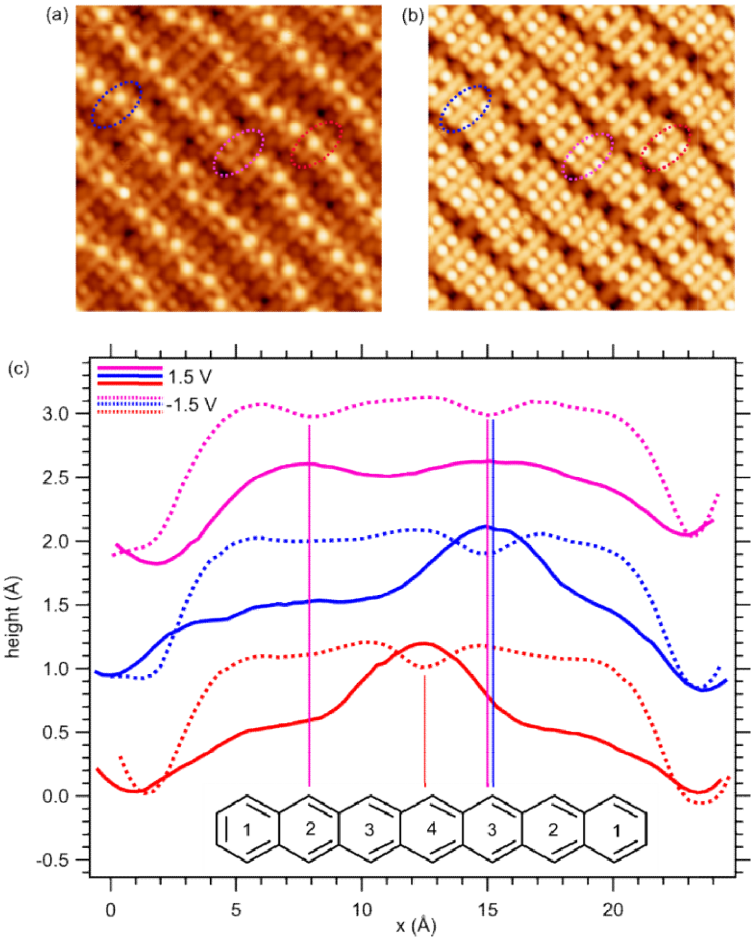

Figure S1. Conventional constant current STM imaging of heptacene intermediates at (a) U = 1.5 V and (b) U = -1.5 V sample bias. The former displays protrusions at the hydrogenated ring, while the latter displays a node. Profiles on the surrounded molecules in (a) and (b) are further displayed in (c), put in relation with a molecular structure model. It can be seen how the same profiles on the same molecules display lobes or nodes at positive or negative bias, respectively, and the correspondence with the particular rings.

Surface morphology variations: comparison between precursors Br-1 and 1 on Ag(001)

The surface morphology resulting from the deposition of precursor Br-1 reveal substantial differences when compared with the one resulting after the deposition of precursor 1. In Figure S1 representative STM images are shown for the deposition of precursor Br-1 (top-panel) and precursor 1 (bottom-panel) on Ag(001) held at RT, for two different coverages: below the 50% of the full terrace area coverage (Θ) (a,c left-panel) and close or above the $\Theta = 50\%$ (b,d right-panel). The trivial difference in the two cases being that the molecules of precursor Br-1 result massively confined in step regions, while precursor 1 predominantly adsorbs on flat regions of the Ag(001) surface.

In Figure S1a an example of surface morphology variation it is shown following the deposition of precursor Br-1 aiming at a coverage $\Theta \leq 10\%$. The flat terraces of Ag(001) remains clean and the molecules are generally found confined in the regions highlighted by the black arrows. A closer analysis of these regions reveals the formation of mono-atomic steps with high density on the Ag(001) surface (see main text Figure 1). By increasing the surface coverage (Figure S1b, $\Theta \geq 50\%$), the extension of the clean flat terraces of Ag(001) is reduced, still, it remain unpopulated by molecules and the extension of the stepped region increases (black arrows highlight a wider region).

The system is notably different when compared with the one resulting from the deposition of precursor 1,a s shown in Figure S1c, since for a comparable coverage as the one of Figure S1a, the molecules are mainly found on the flat terraces of the Ag(001) surface and only decorate the monoatomic step edges. In this system the surface morphology of the Ag the surface morphology is not affected even for higher molecular coverages as show in Figure S1d.

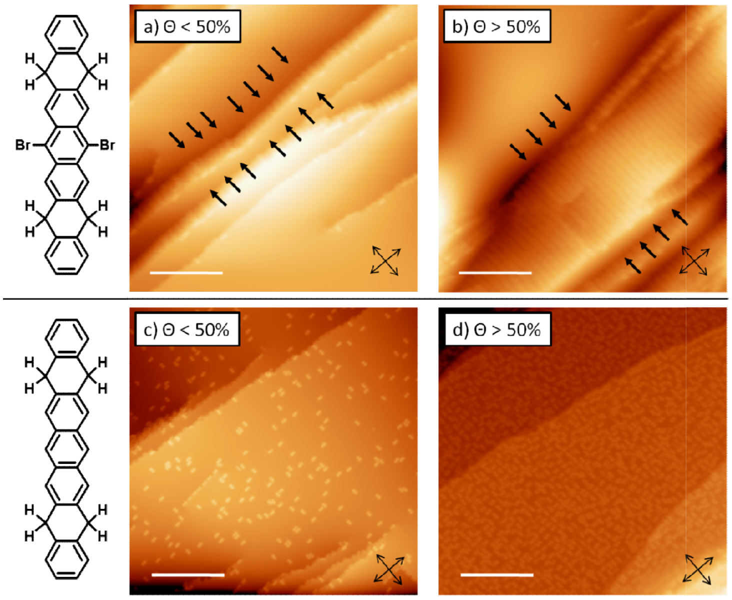

Figure S2: comparison of the surface morphology variations resulting from the deposition of precursor Br-**1** (top) and precursor **1** (bottom) on Ag(001) held at RT, for two different coverages: low (left) and high (right). (a),(b),(c),(d) STM images [scale bar 20nm; all frames recorded at U=1000 mV / I=100pA; 80×80 nm^2]. Square cross arrows represent the high symmetry [110] and [1-10] directions of the substrate. In (a) and (b) black arrows are a guide for the eye used to highlight the extension of the high density step regions at increasing coverages.

Sample after annealing reactant 1 to 180ºC

As opposed to the findings when starting from Br-**1**, displayed in Fig. 3 of the main paper, annealing **1** to 180ºC results in a mixture of tetrahydro, dihydro and fully aromatized molecules in a ratio around 80/13/7. This is exemplified in Fig. S3.

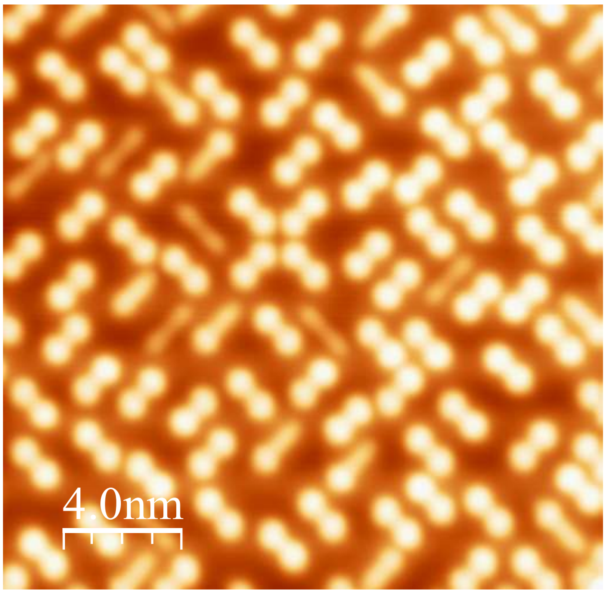

Figure S3: Constant current STM image of a Ag(001) sample after deposition of 1 and subsequent annealing to 180ºC. The tetrahydro, dihydro and fully aromatized molecular species can be discerned from their two bright lobes, one bright lobe, or no lobes together with a lower apparent height, respectively.

Details on calculations

The theoretical electronic structure of gas-phase reactant, intermediates and heptacene molecules have been obtained with the plane-wave package QUANTUM ESPRESSO2[2] using the generalized gradient approximation (GGA) to the exchange-correlation functional in the parametrization of Perdew, Burke, and Ernzerhof (PBE).[3] Ultrasoft pseudopotential[4] with a plane-wave cutoff of 35 Ry for the wave functions and 350 Ry for the charge density were used. All atoms in the molecule were relaxed until forces were smaller than 0.01 eV/ Å.

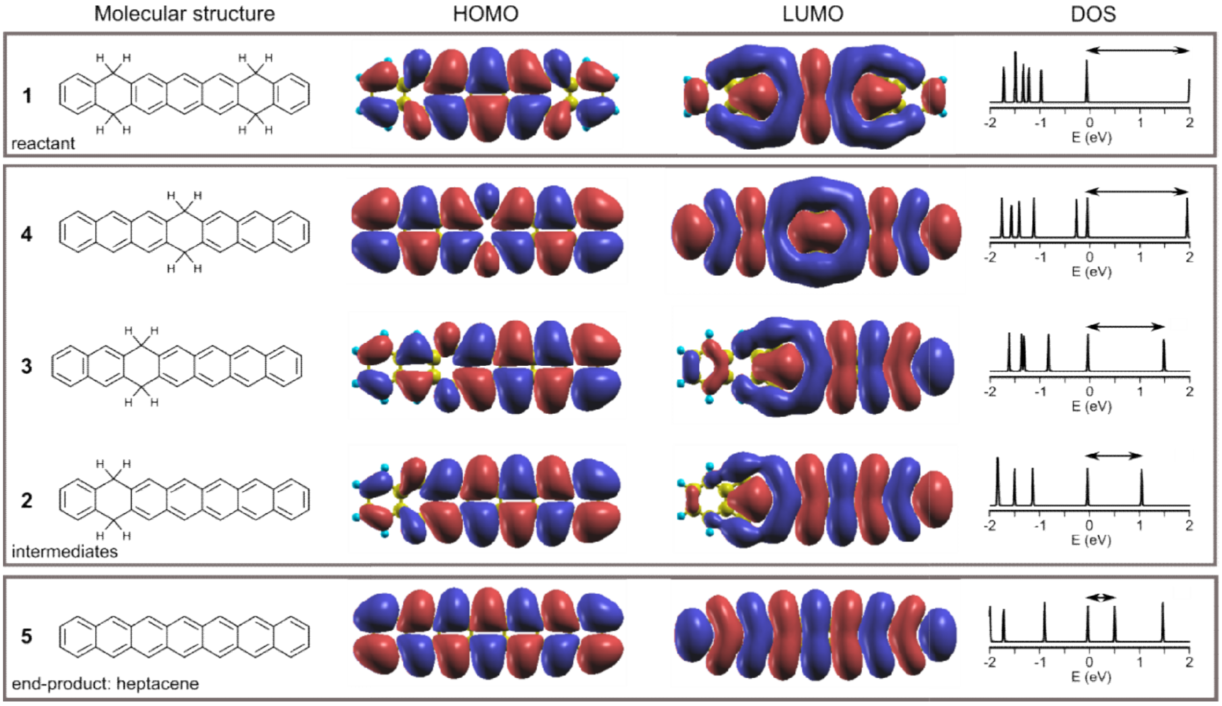

Figure S4. Molecular structure, calculated wavefunctions for gas-phase HOMO and LUMO of reactant, intermediates and product. The right-most column additionally displays the density of states of the respective molecules, with the HOMO level at 0 as reference, revealing how the LUMO shifts to higher energies (increasing the HOMO-LUMO gap, indicated by the arrows) as the longest conjugated segment (which is observed to host most of the HOMO and LUMO density of states) shortens. Interestingly, in line with the experimental observations (Fig. 4 of main text), the gap hardly changes from **1** to **4**, both featuring three rings as the longest conjugated segment.

References

1 R. Dorel, P. R. McGonigal and A. M. Echavarren, *Angew. Chem. Int. Ed.*, 2016, **55**, 11120–11123.

2 P. Giannozzi, O. Andreussi, T. Brumme, O. Bunau, M. Buongiorno Nardelli, M. Calandra, R. Car, C. Cavazzoni, D. Ceresoli, M. Cococcioni, N. Colonna, I. Carnimeo, A. Dal Corso, S. de Gironcoli, P. Delugas, R. A. DiStasio, A. Ferretti, A. Floris, G. Fratesi, G. Fugallo, R. Gebauer, U. Gerstmann, F. Giustino, T. Gorni, J. Jia, M. Kawamura, H.-Y. Ko, A. Kokalj, E. Küçükbenli, M. Lazzeri, M. Marsili, N. Marzari, F. Mauri, N. L. Nguyen, H.-V. Nguyen, A. Otero-de-la-Roza, L. Paulatto, S. Poncé, D. Rocca, R. Sabatini, B. Santra, M. Schlipf, A. P. Seitsonen, A. Smogunov, I. Timrov, T. Thonhauser, P. Umari, N. Vast, X. Wu and S. Baroni, *J. Phys. Condens. Matter*, 2017, **29**, 465901.

3 J. P. Perdew, K. Burke and M. Ernzerhof, *Phys. Rev. Lett.*, 1997, **78**, 1396–1396.

4 We used the pseudopotentials C.pbe.rrjkus.UPF and H.pbe.rrjkus.UPF from the http://www.quantum-espresso.org distribution.